Proceedings of Global Power and Propulsion Society
ISSN-Nr: 2504-4400
GPPS Hong Kong 2023
October 17-19, 2023
www.gpps.global

GPPS-TC-2023-0029

The effects of Reynolds number on the instability boundary and dynamic characteristic of an axial-centrifugal combined compressor

Weihan Kong
Institute for Aero Engine,
Tsinghua University
kwh22@mails.tsinghua.edu.cn
Beijing, China

Jiaan Li
School of Vehicle and Mobility,
Tsinghua University
lja19@mails.tsinghua.edu.cn
Beijing, China

Baotong Wang
Institute for Aero Engine,
Tsinghua University
wangbaotong@tsinghua.edu.cn
Beijing, China

Xinqian Zheng
School of Vehicle and Mobility,
Tsinghua University
zhengxq@tsinghua.edu.cn
Beijing, China

ABSTRACT

The axial-centrifugal combined compressor is the core component of an aero turboshaft engine. The low-Reynolds-number effect caused by the increased flight altitude deteriorates the compressor's stability and restricts the aero-engine's stable working range. This paper numerically investigates the influence mechanism of the Reynolds number on the aerodynamic stability of an axial-centrifugal combined compressor. By establishing a 1D/3D coupling model with the γ-Re_θ turbulent transition model in the 3D flow modelling, the simulation reaches a 2% accuracy of instability boundary prediction, compared with the experimental results. The results show that in the condition of high-Reynolds-number, the instability initiates from the centrifugal stage of the compressor. However, with the decrease of Reynolds number, the component where the instability initiates moves from the last centrifugal stage to the upstream axial stages, which makes the stable working margin drop significantly. Furthermore, the low-Reynolds-number lowers the pressurization capability in the compressor system, which increases the time of the re-pressurization stage in a surge cycle.

INTRODUCTION

When the aero-engine works at a high altitude, the change of the atmospheric environment will affect the working state of the compressor. In order to measure the effect of gas viscosity on compressor performance, the dimensionless Reynolds number (Re) is used to characterize the relative magnitude of gas inertial force and viscous force. With the increasing stage load of advanced aero-engine compressors, a more complex flow field structure appears inside the compressor when the Reynolds number decreases, thus affecting the flow separation phenomenon in the compressor. Furthermore, the flow separation is closely related to the instability of the compressor, thus making the instability boundary of the compressor more sensitive to the low-Reynolds-number effect (Hutchings and Hall, 2021). Therefore, it is an important foundation and support for the design of advanced compressors to reveal the law and mechanism of the Reynolds number's influence on compressors' aerodynamic stability.

At low-Reynolds-number, the compressor's performance, such as pressure ratio, efficiency, mass flow rate, and instability boundary, changes significantly compared to the ground standard Reynolds number. In addition, low-Reynolds-number causes the viscous force of gas to increase, which thickens the internal boundary layer and leads to increased loss, making the flow field structure more complex (Ball et al., 1970; Weigel and Ball, 1972). Therefore, much research has been carried out on the influence mechanism of the low-Reynolds-number effect on compressor performance and stability.

By collecting the test data of nearly 20 axial compressors at different Reynolds numbers, Wassell (1968) proposed the modified formula of Reynolds number for axial compressors, including pressure ratio, efficiency, and surge point's pressure ratio. Based on a large number of test results, Wiesner (1979) made a statistical analysis of the test data of centrifugal

compressors and obtained a modified formula for the influence of the Reynolds number on the mass flow and efficiency of centrifugal compressors. However, this modified formula did not correct the instability boundary of centrifugal compressors. Choi et al. (2008) studied the influence of low-Reynolds-number at high altitudes on the stability of an axial compressor by using three-dimensional numerical simulation. The results showed that low-Reynolds-number affects the boundary layer of the axial compressor, intensifying the boundary layer's flow separation and affecting the compressor's stability. The effect of low-Reynolds-number on the boosting capacity of blades varies with blade height. The total pressure ratio decreases near the blade tip but increases near the root. Cumpsty (2004) wrote in the book that the separation bubble at the leading edge of the blade is a common phenomenon. However, under low-Reynolds-number conditions, the airflow cannot be attached to the blade surface; that is, it is easy to separate, which will deteriorate the stability of the compressor. Wang et al. (2021) conducted numerical simulations of low-Reynolds-number for a cascade, and the study showed that laminar separation bubbles determine the compressor blade losses. With the decrease of Reynolds number, laminar separation bubbles on the suction surface became thicker, and the area of separation area increased. At the same time, it is pointed out that the thickening of the boundary layer caused by low-Reynolds-number will lead to more serious flow blockage and mixing of wake, worsening the efficiency. Zheng et al. (2013) conducted simulations on a transonic centrifugal compressor to reveal the interaction mechanism between boundary layer separation and clearance leakage flow under low-Reynolds-number conditions, and the study showed that the interaction between flow separation and leakage vortex deteriorates the efficiency.

To sum up, many researchers have studied the influence of the Reynolds number on compressor performance, mainly focusing on axial or centrifugal compressors and paying little attention to the influence of the Reynolds number on compressor instability boundary and dynamic characteristics. However, this lacking study is an important basis for understanding the deterioration degree of compressor instability boundary under the low-Reynolds-number. Therefore, in this paper, the axial-centrifugal combined compressor widely used in turboshaft engines is taken as the research object to study the influence of the Reynolds number on the compressor instability boundary, instability mechanism, and surge dynamic characteristics.

METHODOLOGY

Numerical Method

The compression system shown in Figure 1 comprises a compressor, downstream pipe, plenum, and throttle. In order to capture the dynamic characteristics of the compression system during the surge, the simulation model adopted in this paper is one-dimensional-three-dimensional (1D/3D) coupling model. This model adopts the three-dimensional (3D) simulation for the compressor and the one-dimensional (1D) simulation for the pipe, plenum, and throttle downstream.

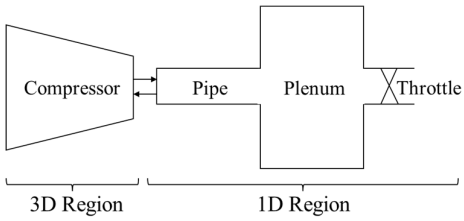

Figure 1 Compression system

The method of characteristics is used to solve the 1D compressible unsteady flow in 1D simulation. The pipe and plenum flow can be regarded as a typical 1D compressible unsteady flow. The ordinary differential equation obtained by the method of characteristics is a physical model describing the propagation of pressure waves and can calculate the transient changes of pressure waves, which has a clear physical significance.

The 3D unsteady model simulates the compressor because there are complex flow phenomena inside the compressor. Moreover, the 3D URANS equation in the compressor fluid domain is solved by the ANSYS CFX solver.

The 1D model adopts the method of characteristics; the iterative variables are mainly Riemann variables, while the boundary conditions of the 3D model are gas state parameters. At the interface of 1D and 3D models, the variables must be transformed in each iteration to realize the information exchange. More details about 1D/3D coupling model can be found in the reference (Huang et al., 2019).

Case Description and Verification

The research object of this paper is an axial-centrifugal combined compressor (Niu, 2021; Zeng, 2022) composed of three axial stages and one centrifugal stage (3A1C). The specific structure includes the inlet guide vane (IGV), first-stage rotor (R1) and stator (S1), second-stage rotor (R2) and stator (S2), third-stage rotor (R3) and stator (S3), and centrifugal impeller (IMP), radial diffuser (DIF-R) and axial diffuser (DIF-A). IGV, S1, and S2 are adjustable, and the meridional view of 3A1C is shown in Figure 2.

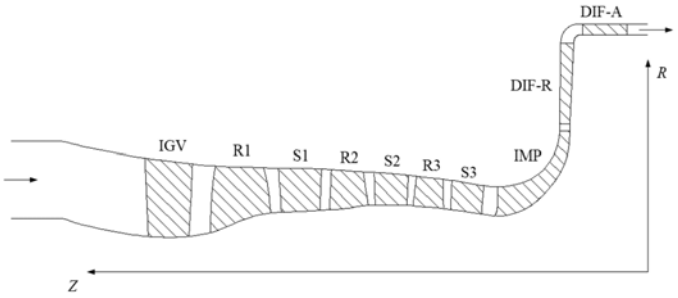

Figure 2 The meridional view of 3A1C

In the 1D/3D coupling model adopted in this paper, the 3D solver is used for solving the 3A1C compressor, while the 1D solver is used for solving the pipe and plenum system behind the outlet of the 3A1C compressor. The compressor characteristics at different altitudes (or *Re*) are simulated by changing the pressure at the inlet of the compression system.

In order to accurately solve the performance of the compressor, the SST turbulence model with γ-Re_θ transition model is selected. The γ-Re_θ transition model is proposed by Menter et al. (2006) and Langtry et al. (2006). This transition model is established based on the empirical formula among the critical momentum thickness Reynolds number of transition, the turbulence intensity, and the pressure gradient of free flow. Moreover, the transport characteristics are utilized to fully consider the influence of free flow on the boundary layer and the momentum thickness Reynolds number transport equation is introduced to avoid using only empirical formula to predict transition. The inlet boundary conditions of the compressor are determined according to the compressor's state. When the gas flows in, the total pressure corresponds to different altitudes, and the total temperature is 288.15K. When the backflow occurs, the inlet pressure should be given static pressure corresponding to different altitudes. The compressor outlet is the interface of the 3D and 1D domains. The interface between the rotor and stator is set as a transient-rotor-stator model, while the interface of DIF-R and DIF-A is set as the mixing plane. The time step of the unsteady calculation is set as 0.00002s, and the number of internal iteration steps is 5. Both numerical schemes for temporal and spatial discretization have second-order precision, and the numerical turbulence scheme adopts a high resolution.

In the 1D simulation, the static pressure at the outlet of the compression system is set as the pressure corresponding to different altitudes, and the working state of the compressor can be changed by adjusting the throttle coefficient. In the 1D simulation domain, the length of pipe L_{out} is 0.1m, the diameter D_{out} is 0.15m, and the volume V_{out} is 0.01m^3.

Mesh independence verification is carried out to validate the mesh model. 5 mesh cases are calculated, and the results are shown in Figure 3.

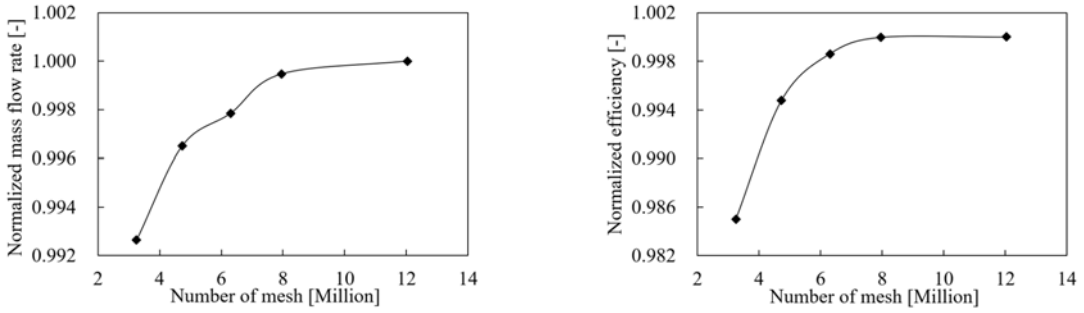

(a) The trend of mass flow rate with mesh number

(b) The trend of peak efficiency with mesh number

Figure 3 Mesh independence verification

As shown in Figure 3, when the number of mesh is greater than 8 million, the mass flow rate and efficiency change are very small. This number has met the mesh independence requirement, so this mesh model is used in the calculation for this paper, which is shown in Figure 4. All the grids are structured, and the boundary layer grids are encrypted to ensure that the y^+ meets the computational requirements of the turbulence model.

Figure 5 shows the dynamic pressure behavior from the numerical and experimental results, when deep surge occurs. Through the comparison between the simulation and experimental results, it can be found that the 1D/3D coupling model can capture the dynamic pressure characteristics during the surge cycle, proving the acceptable accuracy of the numerical method.

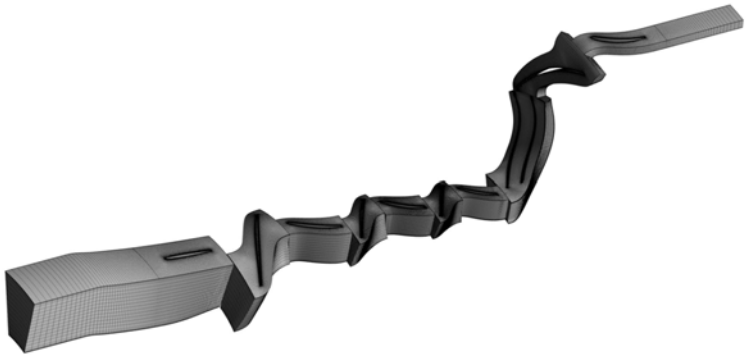

Figure 4 Mesh for calculation

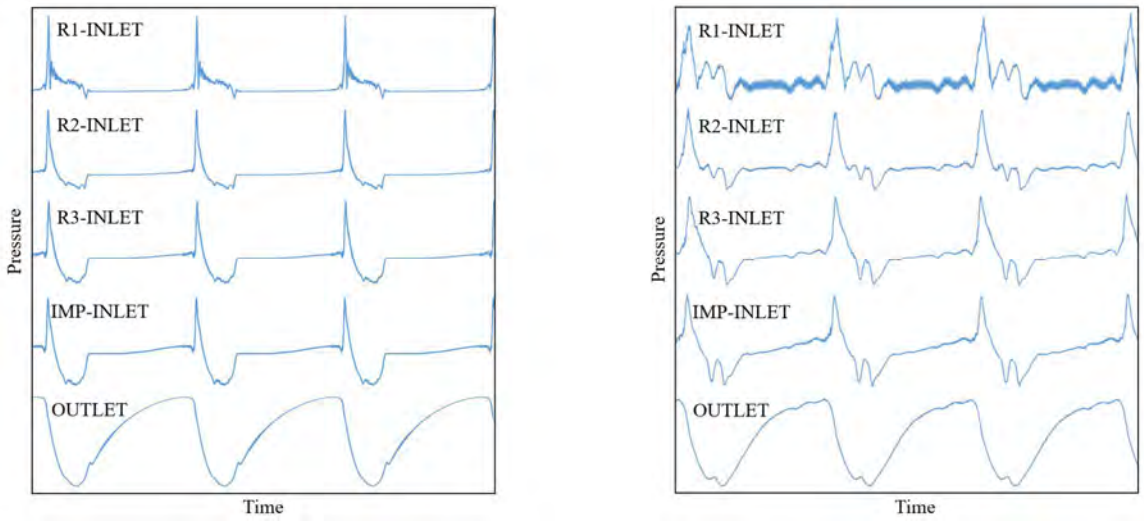

(a) CFD results **(b) EXP results**

Figure 5 The comparison of surge dynamic pressure between CFD and EXP

RESULTS AND DISCUSSION

Effect on the instability boundary

Reynolds number has a great influence on compressor performance and instability boundary. Reynolds number is a dimensionless parameter characterizing the relative magnitude of inertia and viscous forces, and its definition is shown in Equation (1). In addition, to measure the change of instability boundary, the changes in surge point pressure ratio and flow rate are defined respectively, the formula is shown in Equation (2) and (3) :

$$Re = \frac{\rho L_b V_a}{\mu} \qquad (1)$$

$$\Delta\pi = \frac{\pi_{surge} - \pi^*_{surge}}{\pi^*_{surge}} \qquad (2)$$

$$\Delta m = \frac{m_{surge} - m^*_{surge}}{m^*_{surge}} \qquad (3)$$

Where ρ, L_b, V_a, μ represent the airflow density, blade height, airflow axial velocity, and gas dynamic viscosity of the inlet, π_{surge} represents the pressure ratio of the surge point, π^*_{surge} represents the pressure ratio of the referenced surge point, similarly, m_{surge} is the mass flow rate of the surge point, m^*_{surge} is the mass flow rate of the referenced surge point.

The changes of $\Delta\pi$ and Δm with the Reynolds number are shown in Figure 5, which shows Wassell's modified formula (Wassell, 1968), 3A1C compressor test results, and calculation results of the 1D/3D coupling model. From the perspective of trend, the test results are in good agreement with Wassell's modified formula. When the Reynolds number

decreases, the surge point pressure ratio and the mass flow rate decrease, which means that the instability boundary moves to the lower left. When the Reynolds number is in a low range, the surge point pressure ratio and mass flow rate decrease rapidly with the decrease of the Reynolds number. That is, the deterioration of compressor stability is more severe at lower Reynolds number. In addition, by comparing the calculation results of the 1D/3D coupling model with the test results, it can be found that the calculation results of the 1D/3D coupling model accurately predict the compressor's instability boundary and the error is less than 3%, which verifies the accuracy of the 1D/3D coupling model in predicting the instability boundary. It is worth mentioning that the mass flow rate predicted by the 1D/3D coupling model is less sensitive than experiment with the Reynolds number changed, which is also a direction for the coupling model to be further improved.

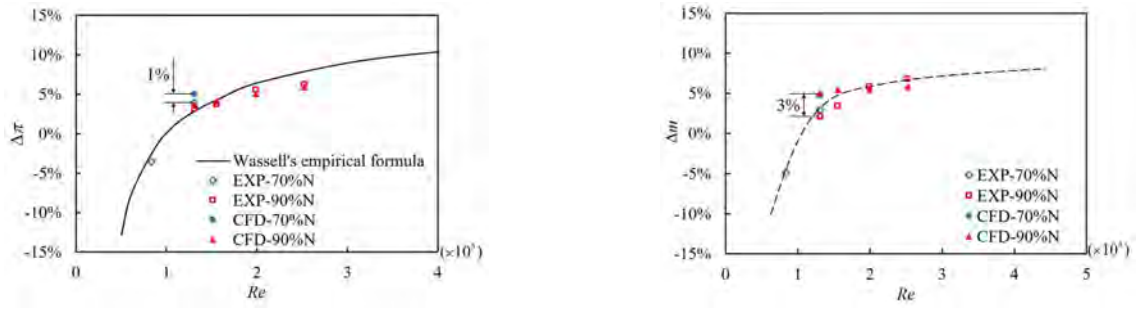

(a) Pressure ratio **(b) Mass flow rate**

Figure 6 Instability boundary under different *Re*

Effect on the near surge characteristic

When the compressor works under the near-surge condition, its internal flows usually separate. Figure 7 shows the Mach number distribution of the compressor under the near-surge condition at an altitude of 0km. Under this condition, a large separation area is generated on the surface of the diffuser blade; thus, the flow is close to instability. As the altitude increases and the Reynolds number decreases, the flow inside the compressor will deteriorate further. In order to explore the influence of Reynolds number on the flow loss of the compressor under the near-surge condition, this section selects some simulation cases of different Reynolds numbers for comparative study, as shown in Table 1. Figure 8 shows the variation of the total pressure loss coefficient of different stages along with the Reynolds number. The total pressure loss coefficient ω is defined as shown in Equation (4), where p_{t_in} and p_{t_out} represent the stator's total inlet pressure and total outlet pressure, and p_{in} represents the static inlet pressure of the stator.

$$\omega = \frac{p_{t\_in} - p_{t\_out}}{p_{t\_in} - p_{in}} \qquad (4)$$

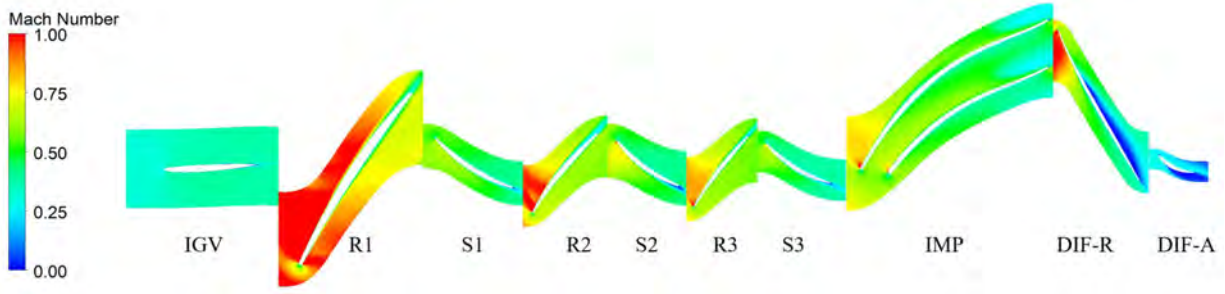

Figure 7 Mach number contour under the near surge condition at 0km (50% span)

$$C_f = \frac{2\tau_w}{\rho_{in} V_{in}^2} \qquad (5)$$

Table 1 Simulation cases for different *Re*

Altitude H [km]	Inlet total pressure P_{t_in} [kpa]	Reynolds number Re [*10^5]
0	100	3.9
4	60	2.3
6	47	1.8
10	26	1.0

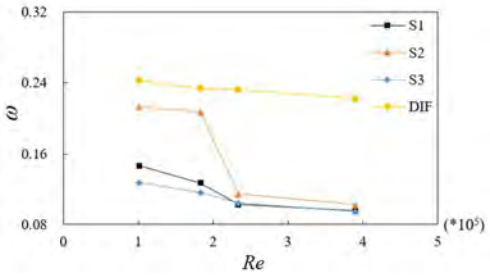

Figure 8 Total pressure loss coefficient of every stator under different *Re*

It can be seen from Figure 8 that the total pressure loss coefficient of every stator increases with the decrease of the Reynolds number, in which the ω corresponding to the diffuser is greater than the stators of the previous three stages under different Reynolds numbers because the diffuser has been separated in a wide range in the near surge condition at the altitude of 0km, so its loss is greater than others. In addition, when the Reynolds number decreases, the loss coefficient of S2 first increases slowly, then rapidly increases to a certain value, and then increases slowly, which may be related to the flow separation on the blade surface. In order to explain the increase in total pressure loss of S2, the wall friction coefficient C_f is defined, and its expression is expressed as Equation (5), where τ_w is the axial shear stress of the wall surface. When $C_f < 0$, it can be considered that the blade surface separation occurrs. Figure 9 and Figure 10 show the distribution of limiting streamlines and wall friction coefficient on the suction surface of S2 at different Reynolds numbers. When Reynolds number decreases, the flow tends to be laminar, and laminar flow has weaker resistance to flow separation than turbulent flow. Therefore, the separation area on the suction surface of S2 gradually increases, and the position of the flow separation point gradually moves to the leading edge, accumulating more low-momentum fluid in the flow passage and reducing the compressor's flow capacity and pressurization capacity. Considering that S2 is an adjustable guide vane, the angle can be appropriately reduced at low-Reynolds-number to prevent a wide range of separation on the suction surface.

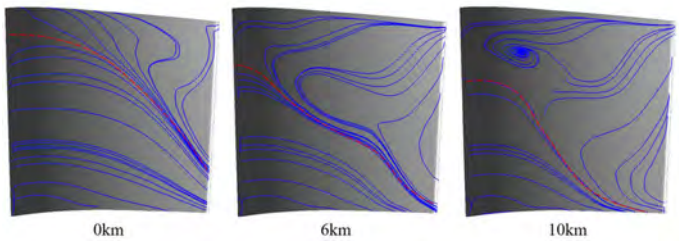

Figure 9 Limiting streamline of S2 suction surface

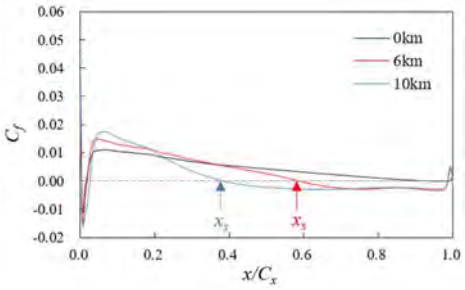

Figure 10 Streamwise distribution of S2's C_f under different *Re* (50% span)

By comparing the wall friction coefficient of other blades, it is found that except for S2, the leading edge of R1 has two closed separation bubbles. According to the discussion by Wang et al. (2021), the position of the laminar separation point (x_s) and turbulent reattachment point (x_r) can be determined by the C_f distribution. As shown in Figure 11, the laminar flow separation point on the R1 pressure surface is basically unchanged under different Reynolds numbers. In contrast, the turbulent reattachment point gradually moves to the trailing edge with the decrease of Reynolds number. On the suction surface, with the decrease of Reynolds number, the laminar separation point moves to the leading edge, and the turbulent reattachment point gradually moves to the trailing edge. The same rule applies in different spanwise locations. With the decrease of Reynolds number, the increase of separation bubble will lead to the increase of the downstream boundary layer thickness and the accumulation of more low-momentum fluid at the trailing edge, leading to the deterioration of compressor performance.

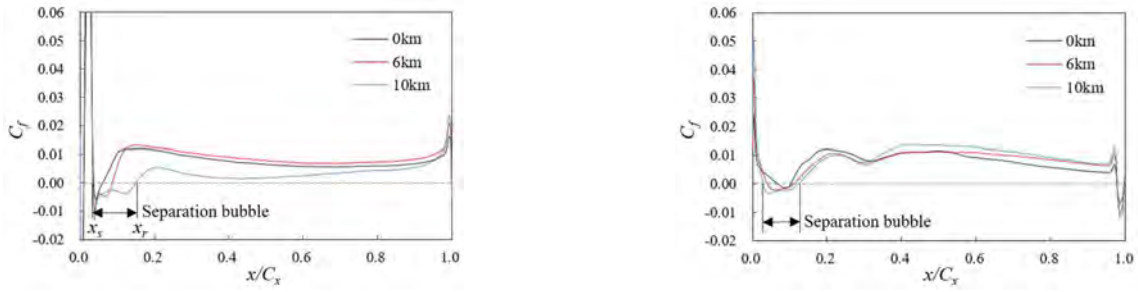

(a) Pressure surface **(b) Suction surface**

Figure 11 Streamwise distribution of R1's C_f under different *Re* (50% span)

Effect on the dynamic characteristic of surge

In order to capture the complete surge process and analyze the dynamic characteristics, the turbulence model in this section is set as the $k-\varepsilon$ model, which has been verified by experiments in the study (Li et al., 2022).

Figure 12 compares the changes in mass flow rate and static pressure of the plenum during surge under two typical working conditions with 0km and 6km altitude. The Reynolds number corresponding to the two working conditions is 3.9×10^5 and 1.8×10^5, respectively. The variation trend of mass flow rate and pressure under the two Reynolds numbers are basically the same, though the time of a surge cycle is different. The time of a surge cycle under the large Reynolds number is 0.09152s, and the frequency is 10.93Hz. However, the time of a surge cycle under the low-Reynolds-number is 0.17004s, and the frequency is 5.88Hz.

In order to further compare the difference in the time of a surge cycle, the compressor surge process is divided into four stages (Cumpsty, 2004). The stage ① is the flow collapse stage, which starts from the maximum static pressure ratio point and ends at zero mass flow rate point. The stage ② is the reverse stage, in which the mass flow rate is always negative; The stage ③ is the recovery stage, starting from the point of zero mass flow rate to the point where the mass flow rate reaches the top; The stage ④ is the re-pressurization stage, which includes the re-pressurization of the compressor along the characteristic line to the maximum pressure ratio point. The static pressure of the plenum corresponding to the ①, ②, and ③ stages decreases, and the plenum is in the empty process. On the other hand, the static pressure of the plenum corresponding to the ④ stage rises, and the plenum is in the filling process. As can be seen from the comparison of the corresponding time of the four surge stages in Figure 13, with the decrease of Reynolds number, the time of the ①, ②, and ③ stages slightly increases, while the time of the ④ stage increases significantly. The change in the time of a surge cycle can be explained by the definition of the Reynolds number, which represents the relative magnitude of inertia force and viscous force. When the Reynolds number decreases, the ratio of inertia force and viscous force decreases, which reduces the speed of filling and empty process in the plenum, and thus increases the surge period. In addition, it can be seen from the comparison of surge cycles in Figure 13 that the maximum pressure ratio achieved by the compressor under the low-Reynolds-number is less than the maximum pressure ratio under the high-Reynolds-number, that is, with the decrease of Reynolds number, the pressurization capacity of the compressor decreases, which also explains why the time of re-pressurization stage decreases with the decrease of Reynolds number.

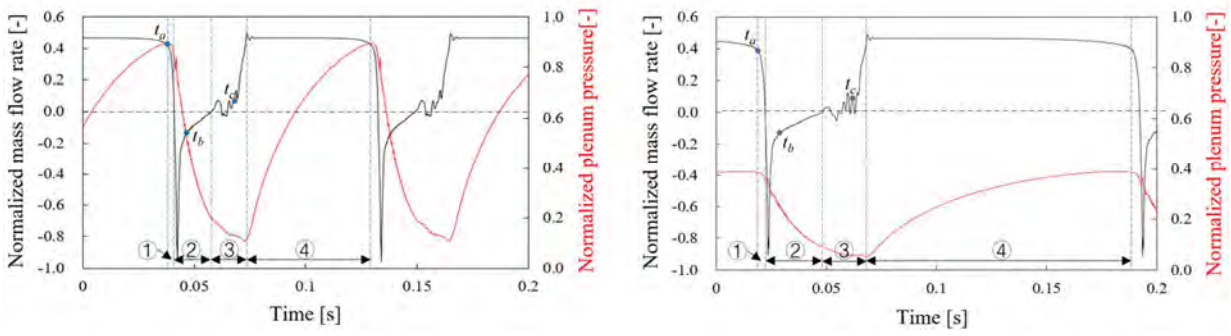

(a) 0km **(b) 6km**

Figure 12 Comparison of surge process (The black line shows the change of corrected mass flow rate and the red line shows the change of plenum pressure.)

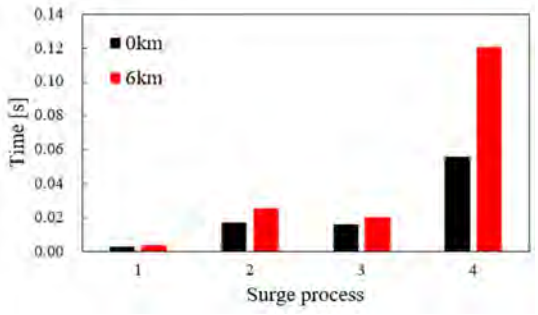

Figure 13 Comparison of surge time

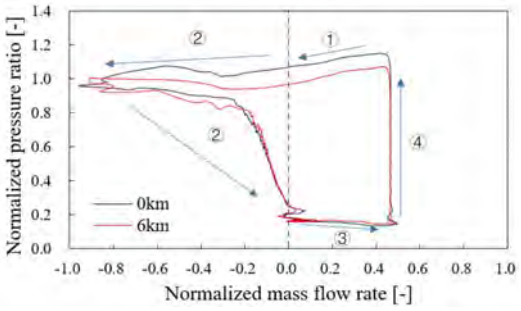

Figure 14 Comparison of surge cycle

During a surge cycle, there are generally four stages, among which the flow field analysis in the re-pressurization stage is common and will not be conducted in this paper. In the other three stages, three typical moments marked in Figure 12 are selected for comparative analysis on the flow field. Figure 15 shows the axial velocity contours of meridional view at the different moment of a surge cycle. At the starting moment of flow collapse stage marked by ①, the axial velocity is basically positive, but the velocity in the passage of radial diffuser is quite low, indicating the existence of a strong separation. The tip leakage flow can also be observed near the tip of rotors and hub of stators . Also, it can be clearly seen that with the decrease of Reynolds number, the tip leakage flow at the tip of R1 enhances. As the flow is reversed as shown in Figure 15(b), there is a quite clear reverse flow region upstream the compressor. Furthermore, when the Reynolds number decreases, the absolute velocity of this reverse flow region increases, representing the enhancement of flow reversal. At the recovery stage in Figure 15(c), the flow reversal is alleviated, and the compressor is gradually returning to the choke condition. The reverse flow is mainly found near the tip of rotors and hub of stators, and with the decrease of Reynolds number, the tip leakage flow gets strong at the corresponding region.

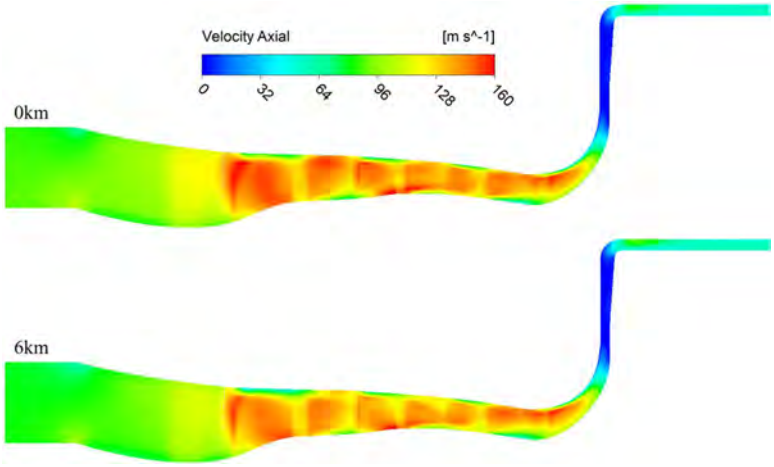

(a) t_a - flow collapse stage

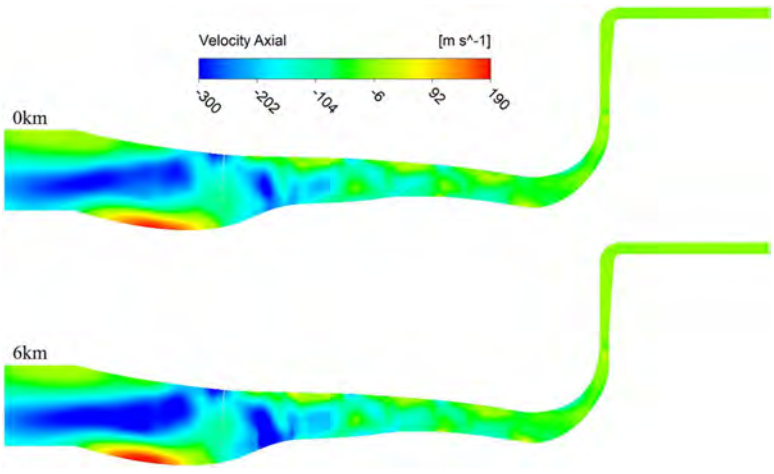

(b) t_b - reverse stage

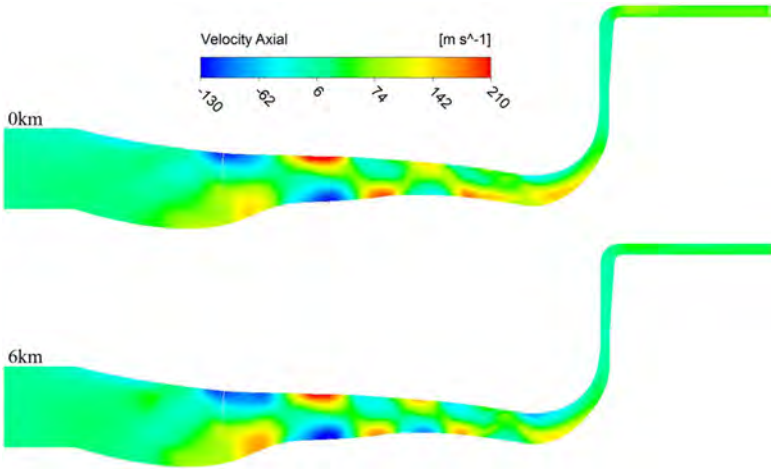

(c) t_c - recovery stage

Figure 15 Axial velocity contours of meridional view at different time of a surge cycle

CONCLUSIONS

In this paper, a multistage axial-centrifugal combined compressor is taken as the research object, and the 1D/3D coupling model is used to investigate the flow behavior of a 3A1C combined compressor with changed inlet Reynolds number. First, the Reynolds number's influence on the compressor's instability boundary is studied. Next, the influence law and mechanism of the flow characteristics of instability inception with changed Reynolds number is revealed. Finally, the Reynolds number's influence on the dynamic characteristics of the surge is analyzed. The main conclusions of this paper are drawn as follows:

(1) The comparison with the experimental results shows that the 1D/3D coupling model using the γ-Re_θ transition model can accurately predict the compressor instability boundary, and the error is less than 2%; With the decrease of Reynolds number, the pressure ratio at the instability point of compressor first slowly decreases and then rapidly decreases. At 70% rotating speed, the pressure ratio and flow rate at the instability point decrease by about 8% when the Reynolds number decreases from 1.3×10^5 to 0.8×10^5, indicating that the influence of the Reynolds number on the compressor instability boundary cannot be ignored.

(2) The decrease of Reynolds number leads to the deterioration of blade resistance capability to separation, the separation position on the blade moves forwards to the leading edge, and the separation area becomes larger and expands to more stages. Moreover, the closed separation bubbles are found on the pressure and suction surfaces of R1. The separation bubble grows with the decrease of Reynolds number, and the reattachment position moves downstream to the trailing edge. All these factors lead to the accumulation of a large amount of low-momentum fluid in the flow passage at low-Reynolds-number, which deteriorates the compressor performance due to the loss and blockage.

(3) When Reynolds number decreases, the ratio of inertial force to viscous force decreases, which reduces the speed of filling and empty process in the plenum, causing that the surge period increases and the surge frequency decreases; Moreover, due to the decrease of the compressor's boosting capacity caused by the low-Reynolds-number, the time of re-pressurization becomes significantly longer, which also enlarges the surge period. In a surge cycle, the flow reversal abruptly gets strong at the beginning of flow collapse stage. Then, at the recovery stage, the reverse flow gradually becomes weak until the compressor is back to the choke condition. Additionally, the obvious difference between the flow fields from the results of two Reynolds number is the strength of flow reversal at the reverse stage. With the decrease in Reynolds number, the reverse flow clearly enhances.

NOMENCLATURE

C	Blade chord	Re	Reynoldes number	μ	Dynamic viscosity
C_f	Skin friction coefficient	V	Volume or velocity	π	Pressure ratio
m	Mass flow rate	x	Streamwise distance	ω	Total pressure loss coefficient
p	Pressure	ρ	Density	τ	Shear stress

Superscript

*	Reference point

Subscripts

a	Axial	*r*	Reattachment point	*w*	Wall surface
b	Blade	*s*	Separation point	*x*	Streamwise coordinate
cor	Corrected parameter	*t*	Stagnation parameter		

Abbreviations

1D/3D	One-dimensional-three-dimensional
3A1C	Three-stage axial and one-stage centrifugal combined compressor
URANS	Unsteady Reynolds-Averaged Navier-Stokes Method

ACKNOWLEDGMENTS

This research was supported by the National Major Science and Technology Project of China [No. 2017-II-0004-0016].

References

Ball, C., Heidelberg, L. and Weigel C. (1970). Effect of Reynolds number on overall performance of a 6-inch radial bladed centrifugal compressor. NASA TN D-5761.

Choi, M., Baek, J. H., Chung, H. T., Oh, S. H. and Ko, H. Y. (2008). Effects of the low Reynolds number on the loss characteristics in an axial compressor. *Proceedings of the Institution of Mechanical Engineers, Part A: Journal of Power and Energy*, 222(2), pp. 209-218.

Cumpsty, N. A. (2004). *Compressor Aerodynamics*. Florida.

Huang, Q. Q., Zhang, M. J. and Zheng, X. Q. (2019). Compressor Surge Based on a 1D-3D Coupled Method — Part I: Method Establishment. *Aerospace Science and Technology*, 90, pp. 342-356.

Hutchings, J. and A. Hall, C. (2021). The Effects of Reynolds Number on the Stall and Pre-Stall Behavior of Compact Axial Compressors. *Journal of Turbomachinery*, 143(12), 121014.

Langtry, R. B., Menter, F. R., Likki, S. R., Suzen, Y. B., Huang, P. G. and Völker, S. (2006). A correlation-based transition model using local variables—part II: test cases and industrial applications. *Journal of turbomachinery*, 128(3), pp. 423-434.

Li, J., Wang, B., Yang, H., Fan, T., Song, Z., Wang, J. and Zheng, X. (2022). Investigation on probe streamwise distribution for surge measurement in compression system. *Aerospace Science and Technology*, 108009.

Menter, F. R., Langtry, R. B., Likki, S. R., Suzen, Y. B., Huang, P. G. and Völker, S. (2006). A correlation-based transition model using local variables—part I: model formulation. *Journal of turbomachinery*, 128(3), pp. 413-422.

Niu, Z. (2021). *Effects and Mechanisms of Low Reynolds Number on Compressors' Flow Stability*. M.D. Tsinghua University.

Wang, M., Lu, X., Yang, C., Zhao, S. and Zhang, Y. (2021). Numerical investigation of distributed roughness effects on separated flow transition over a highly loaded compressor blade. *Physics of Fluids*, 33(11), 114104.

Wassell, A. B. (1968). Reynolds Number Effects in Axial Compressors. *ASME. J. Eng. Power*, 90(2), pp. 149-156.

Weigel, C. and Ball, C. (1972). Reynolds number effect on overall performance of a 10.8-centimeter (4.25-inch) sweptback bladed centrifugal compressor. NASA TN D-6640.

Wiesner, F. (1979). A new appraisal of Reynolds number effects on centrifugal compressor performance. *Transactions of the ASME*, 101, pp. 384-392.

Zeng, H. (2022). *Research on the Analytical Method and the Mechanisms of Aerodynamic Instability in Aero-Engines*. Ph.D. Tsinghua University.

Zheng, X., Lin, Y., Gan, B., Zhuge, W. and Zhang, Y. (2013). Effects of Reynolds number on the performance of a high pressure-ratio turbocharger compressor. *Science China Technological Sciences*, 56, pp. 1361-1369.